

The core size of the Fornax dwarf Spheroidal

N. C. Amorisco^{1*}, A. Agnello¹ and N. W. Evans¹

¹*Institute of Astronomy, University of Cambridge, Madingley Road, Cambridge CB3 0HA, UK*

Accepted, Received

ABSTRACT

We exploit the detection of three distinct stellar subpopulations in the red giant branch of the Fornax dwarf Spheroidal to probe its density distribution. This allows us to resolve directly the evolution with radius of the dark matter mass profile. We find that a cored dark matter halo provides a perfect fit to the data, being consistent with all three stellar populations well within 1-sigma, and for the first time we are able to put constraints on the core size of such a halo. With respect to previous work, we do not strengthen the statistical exclusion of a dark matter cusp in Fornax, but we find that Navarro-Frenk-White haloes would be required to have unrealistically large scale radii in order to be compatible with the data, hence low values of the concentration parameter. We are then forced to conclude that the Fornax dwarf Spheroidal sits within a dark matter halo having a constant density core, with a core size of $r_0 = 1_{-0.4}^{+0.8}$ kpc.

Key words: galaxies: kinematics and dynamics – Local Group – galaxies: individual; Fornax dSph

1 INTRODUCTION

Dynamical modelling of the dwarf Spheroidals (dSphs) has now been tackled with a number of different techniques. At the heart of these efforts lies the importance of constraining the properties of the central dark matter density profile, so as to advance our understanding of galaxy formation towards the low-mass end of the mass-spectrum. Jeans equation analyses (e.g. Walker et al. 2009b; Lokas 2009), phase-space analyses (Wilkinson et al. 2002; Wu 2007; Amorisco & Evans 2011) as well Schwarzschild modelling (Jardel & Gebhardt 2012; Breddels et al. 2012) have all now been used in this field, with varied degrees of success. Nonetheless, it is fair to say that the main step forward has not really come through brute force in the modelling techniques, but rather from the realization that the presence of multiple stellar populations in dSphs could be turned into a powerful strength.

After the first work of Battaglia et al. (2008), the method has now been amplified to overcome some of the deficiencies of Jeans analyses (Evans et al. 2009; Amorisco & Evans 2012a) and to give the required robustness to the identification and disentanglement of the co-existing stellar subpopulations (Walker & Peñarrubia 2011, WP11 in the following). Very recently, Agnello & Evans (2012) (AE12) have brought the argument into sharp focus. They show that the additional evidence coming from co-existing subpopulations is extremely simple in nature, and

can be fully understood in terms of the independent requirements to the global energetics of the system enforced by the different stellar subpopulations. By using the projected virial theorem (PVT) it is possible to identify the dark matter profiles that are compatible with the photometry and kinematics of the subpopulations and exclude those in which the subpopulations would not all be in equilibrium at the same time.

New rich and precise datasets will certainly allow and justify full use of more refined dynamical techniques in the near future, especially exploiting the spatially resolved properties of the line of sight (LOS) velocity distribution (Amorisco & Evans 2012b; Jardel & Gebhardt 2012, JG12 in the following). On the other hand, while the detailed orbital distribution of the stars is still a major uncertainty in the modelling, it is helpful to work within a framework that is entirely free from any anisotropy-driven degeneracy, such as the PVT.

All the analyses mentioned so far point towards the presence of a constant density core at the center of both studied dSphs, Sculptor and Fornax. Together with previous evidence pertaining to low surface brightness galaxies (e.g. de Blok et al. 2001), these results have triggered a number of both theoretical and numerical studies. The aim is of course to understand the complex baryonic processes responsible for transforming the initial dark matter $\rho \sim r^{-1}$ cusp predicted by Cold Dark Matter (CDM) models (Dubinski & Carlberg 1991; Navarro et al. 1997)

$$\rho_{\text{NFW}}(r) = \frac{\rho_0}{\left(\frac{r}{r_0}\right) \left(1 + \frac{r}{r_0}\right)^2} \quad (1)$$

* E-mail: amorisco@ast.cam.ac.uk, aagnello@ast.cam.ac.uk, nwe@ast.cam.ac.uk

into a core. A number of suggestions have been made, including multiple epochs of mass loss and gas re-accretion (Read & Gilmore 2005), clumpy baryonic infall (Cole et al. 2011) and intermittent and concentrated star formation and subsequent supernova feedback (Pontzen & Governato 2012). Some or all of these processes may be able to deposit sufficient energy in the dark matter halo to erase the central cusp. This picture has been tested with promising results by Teyssier et al. (2012) and Brooks & Zolotov (2012), who show that a more realistic treatment of star formation and feedback can reduce the tension between CDM and the detection of cores in luminous dSphs.

In this *Letter*, we revisit the dark matter density profile of the Fornax dSph, after Amorisco & Evans (2012c) (A12) found that a three-population division better describe the data with respect to a two-population division (WP11). Both previous analyses of the Fornax dSph (WP11, JG12) were able to exclude the presence of an Navarro-Frenk-White (NFW) cusp with high statistical significance, although the size of the constant density core has remained poorly constrained. WP11 obtain a measurement of the average logarithmic slope of the mass profile Γ (see eqn. (4)) at a radius that is comparable with the half-light radii of their two subpopulations. This only allows them to put a lower limit to the core size. Similarly, JG12 find that a constant density core is required, but orbit-based modelling of a single stellar population would require a more extended set of kinematic tracers in order to put an upper limit to its scale length. By exploiting all the three different stellar populations in Fornax, we are able to find such a constraint.

2 PROBING THE MASS PROFILE

A12 present evidence for the coexistence of three distinct stellar subpopulations in the red giant branch of the Fornax dSphs. These subpopulations have different metallicities, spatial distributions and kinematics. We refer to their Table 1 for details, and record here for convenience the relevant half-light radii:

$$\begin{cases} R_h^{\text{MP}} &= 935 \pm 65\text{pc}, \\ R_h^{\text{IM}} &= 610 \pm 25\text{pc}, \\ R_h^{\text{MR}} &= 437 \pm 55\text{pc}, \end{cases} \quad (2)$$

where MP, IM and MR stand, respectively, for metal-poor, intermediate-metallicity and metal-rich. Fig. 1 displays the LOS velocity dispersion profiles of the three stellar subpopulations. These have been obtained by using the maximum likelihood technique described in Amorisco & Evans (2012b), which takes into account the probabilities of membership of each star to the identified stellar subpopulations.

With this information, we produce a total mass estimate for each subpopulation. We use the mass estimator proposed by Amorisco & Evans (2012a)

$$M [(1.67 \pm 0.04)R_h] = (5.85 \pm 0.2) \frac{R_h \sigma_{\text{los}}^2(R_h)}{G}, \quad (3)$$

which has been proved to be accurate on the wide family of models with Michie-King phase space distribution. We also notice that use of alternative mass estimators with the

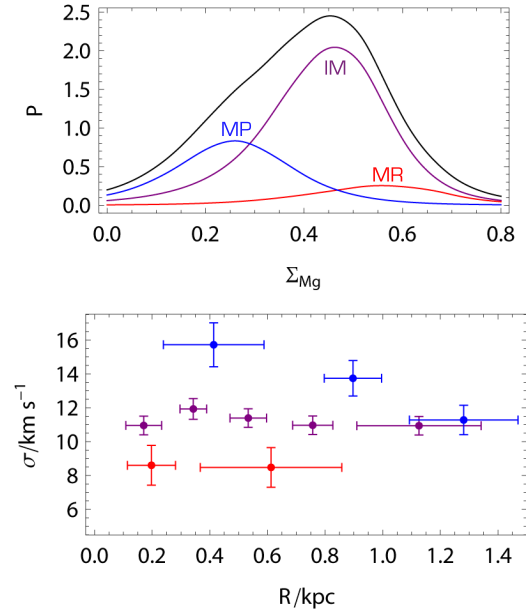


Figure 1. Metallicity distribution (in the Magnesium index – in Å) and line of sight velocity dispersion profiles in circular annuli for the three stellar subpopulations identified in Fornax. Color-coding corresponds to increasing metallicity. The profiles use the same number of tracers per bin, although this is different for each population (34 for MR, 283 for IM and 123 for MP).

same functional structure – as for example the one proposed by Walker et al. (2009b) and used in WP11 – would give identical results for the logarithmic slope of the mass profile

$$\Gamma_{i,j} = \frac{\log M_i - \log M_j}{\log R_{h,i} - \log R_{h,j}}, \quad (4)$$

where i and j identify any two stellar subpopulation. The left panel of Fig. 2 illustrates the one and two sigma contours for each of the total mass estimates, with the same color-coding as in Fig. 1; the right panel of the same Figure shows the probability distributions of the three logarithmic slopes obtained by combining in pairs the distinct subpopulations.

For any realistic dark matter density profile, the logarithmic slope $\Gamma(r)$ is a monotonic function of radius and decreases to zero at large radii. For a cored halo, $\Gamma \lesssim 3$ within the scale radius of the core. For a cusped dark matter profile $\rho \sim r^{-\gamma}$, $\Gamma \lesssim 3 - \gamma$ near the center. Therefore, for an NFW halo, Γ is never higher than 2. WP11 have measured a value of Γ that is systematically higher than 2 near the center of Fornax, and were able to exclude the presence of a cusp ($\gamma \geq 1$) with high significance ($s \geq 96\%$). Since we have three different mass estimates, we can measure the logarithmic slope of the mass profile in multiple locations, hence assess directly its evolution with radius. In the radial interval defined by the IM and MP stellar populations, which is the farthest from the center, the slope is centered on $\Gamma \approx 2$ (blue-purple curve in the right panel of Fig. 2). However, as soon as the radius is reduced by considering the MR stellar population, the mean value of Γ systematically increases. By considering the MR-MP pair (red-blue curve) we obtain $\langle \Gamma \rangle \approx 2.4$, while, near the center, the MR-IM pair (red-purple curve) suggests $\langle \Gamma \rangle \approx 2.65$. This is probing directly the radial variation of the mass profile of the Fornax dwarf.

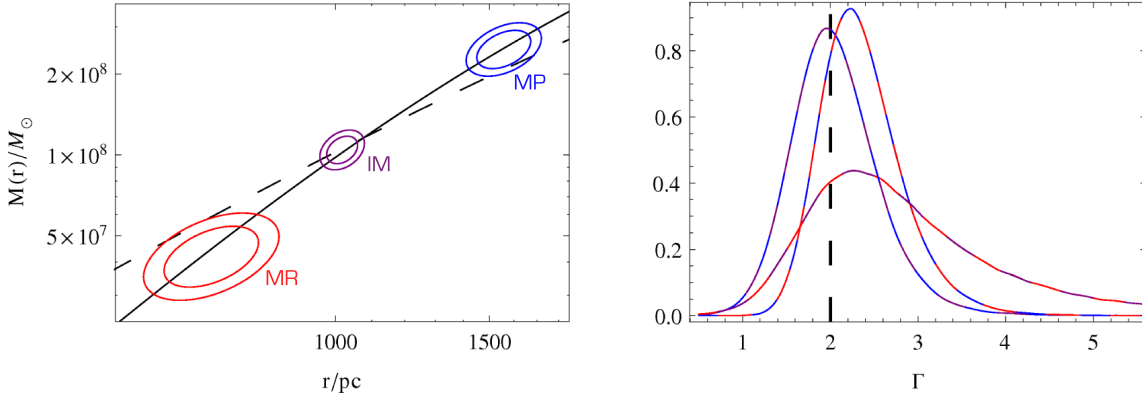


Figure 2. Left panel: estimates of the total enclosed mass $M(r)$ as obtained from each of the three stellar subpopulations; color-coding is the same as in Fig. 1. Right panel: probability distributions of the logarithmic slope Γ obtained by pairing the mass estimates in the left panel (colors are paired accordingly).

In a purely statistical sense, the exclusion of an NFW cusp we obtain from this analysis is not as strong as the one obtained in WP11: the tails of the probability distributions of both $\Gamma_{\text{MR,MP}}$ and $\Gamma_{\text{MR,IM}}$ suggest that the probability of a density profile as steep or steeper than an NFW is $p \lesssim 22\%$. Nonetheless, it is worth noticing that such a cusped density profile would be unrealistic for different reasons. For instance, the dashed fitting curve in the first panel of Fig. 2 represents the best fitting NFW halo with scale radius $r_0 = 3$ kpc. The agreement with the mass estimates is marginal and it is in fact impossible to obtain a better agreement for any NFW density profile with a smaller scale radius (hence even smaller $\langle \Gamma \rangle$ at the same radii). Different studies of Fornax (Irwin & Hatzidimitriou 1995; Cole et al. 2012, WP11) suggest that its tidal radius is likely to be smaller than 3 kpc, hence presenting an evident incompatibility with the required scale radius. Furthermore, even an NFW halo with a scale radius of ‘only’ $r_0 > 2$ kpc would already have a concentration $c < 9$, well below the expectation of CDM models (e.g. Macciò et al. 2007). As a comparison, the full line in the left panel of Fig. 1 represents a Burkert profile (Burkert 1995)

$$\rho_{\text{Bur}}(r) = \frac{\rho_0}{\left(1 + \frac{r}{r_0}\right) \left[1 + \left(\frac{r}{r_0}\right)^2\right]} \quad (5)$$

with a core-size of $r_0 \approx 1.4$ kpc, which provides excellent agreement with the mass estimates, being consistent with all three stellar populations well within 1-sigma.

3 PROJECTED VIRIAL THEOREM

We can gain a more systematic insight by making use of the PVT

$$2K_{\text{los}} + W_{\text{los}} = 0, \quad (6)$$

where, in the usual notation, K_{los} and W_{los} are the projected components of the pressure and potential energy tensors – explicit formulæ are recorded in AE12. The PVT provides a fundamental means of exploring the energetics of a system with multiple stellar subpopulations. As in AE12, we assume that the photometry of the different subpopulations is well

represented by a Plummer profile; we have performed the same analysis using exponential profiles and find consistent results.

In the ideal case of no observational uncertainties, use of the PVT proceeds as follows. For an assigned dark matter density profile, once the surface brightness of a stellar subpopulation $\mu(r)$ and its velocity dispersion profile $\sigma_{\text{los}}(r)$ are given, the PVT yields the characteristic density ρ_0 that needs to be coupled with the scale radius r_0 in order to have an equilibrium configuration. In our application, we use a Monte Carlo procedure to propagate any observational uncertainties in the half-light radius of the photometry from eqn. (2) as well as in the kinematics (see Fig. 1), and construct a complete probability distribution for the characteristic density ρ_0 at any fixed characteristic radius r_0 .

The left panel of Fig. 3 shows the one-sigma virial stripes that we obtain when each subpopulation is embedded in an NFW dark matter profile (eqn. (1)); the right panel illustrates the case of a Burkert halo (eqn (5)). In the NFW case, the one-sigma regions related to the IM and MP subpopulations overlap before $r_0 = 1$ kpc. This is in agreement with the previous Section, since we found $\langle \Gamma_{\text{MR,IM}} \rangle = 2.0$ at large radii. However, at smaller radii the MR subpopulation does not fit into this picture. Any NFW halo that is compatible at the one-sigma level with all three subpopulations has $r_0 \gtrsim 2$ kpc, with the difficulties mentioned earlier. On the other hand, for a constant density core, the three one-sigma stripes show a consistent overlap region.

Use of a single subpopulation does not allow any inference on the scale radius of the core if taken by itself. It is by multiplying the probability distributions defined by the three virial stripes that we can constrain the core size. Fig. 4 displays the one- and two-sigma confidence regions associated with the joint likelihood, together with the marginalized probability distributions for the characteristic density ρ_0 and core size r_0 . All full lines are associated with a Burkert dark matter profile (eqn. (5)), but we find that the data do not show any significant preference for other functional prescriptions of the core. For example, we have explored the density profile used by AE12

$$\rho_{\text{cNFW}}(r) = \frac{\rho_0}{\left[1 + \left(\frac{r}{r_0}\right)^2\right]^{3/2}} \quad (7)$$

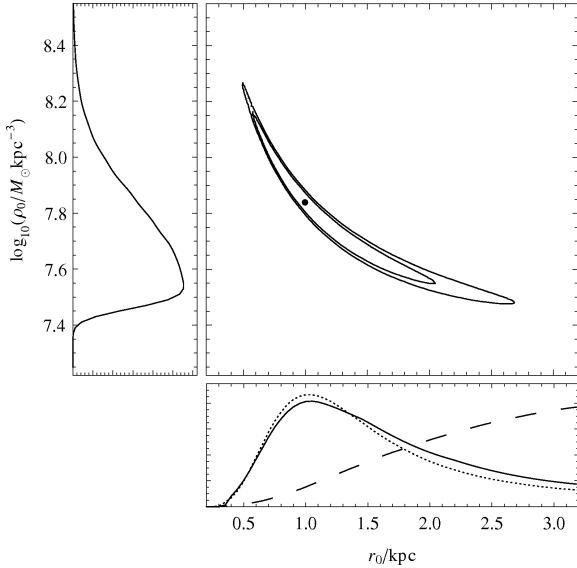


Figure 4. Joint likelihood analysis of the virial stripes: one and two sigma contours in the halo plane ($r_0; \rho_0$) and marginalized probability distributions for a Burkert density profile (full lines). The short-dashed probability distribution is associated with the cored profile of eqn. (7), while the long-dashed distribution is indicative of an NFW halo.

and we find no difference in either the virial stripes or in the maximum value of the joint likelihood. In fact, the dotted line in the lower panel of Fig. 4 has been obtained by using the density profile (7), but this is virtually indistinguishable from the one obtained for a Burkert profile. As a comparison, the dashed line in the same panel is associated with the joint likelihood of an NFW halo. Increasing the scale radius r_0 is the only way to increase the average value of Γ in the radial region sampled by the three stellar subpopulations, therefore the marginalized probability distribution is a monotonically increasing (respectively, decreasing) function of r_0 (of c). We then conclude that the 68% confidence interval for the core size is $r_0 = 1_{-0.4}^{+0.8}$ kpc.

4 CONCLUSIONS

The Fornax dwarf is the brightest, and probably the most massive of all the dwarf spheroidal (dSph) companions surrounding the Milky Way Galaxy. It has a complex evolutionary pathway, as is already evident from its star formation history (Coleman & de Jong 2008; de Boer et al. 2012). The detection of localized overdensities (Coleman et al. 2004, 2005) as well as a complex dependence on metallicity of its rotational properties (Amorisco & Evans 2012c) support the idea of a relatively recent interaction with a smaller dwarf. Large spectroscopic samples of thousands of red giant stars in Fornax are now available (Walker et al. 2009a), and have recently been separated into three populations – metal-rich, intermediate-metallicity and metal-poor – by Amorisco & Evans (2012c) using chemo-dynamical methods.

In stellar dynamics, multiple populations provide a powerful method to constrain the common gravitational potential in which the stars move. Here, we have exploited the

division of Fornax into three populations to show that the stars reside in a dark matter halo having a constant density core with size of $r_0 = 1_{-0.4}^{+0.8}$ kpc. This is in contrast to the case when just the single, combined stellar population of Fornax is studied. Then, the kinematic data are equally consistent with cusps and cores (Evans et al. 2009; Strigari et al. 2010). Although often cited as an issue, the ellipticity of the luminous dSphs is unable to alter the conclusions on their dark matter density profiles, as shown by Agnello & Evans (2012). Even an oblate NFW halo would still need to be so large and diffuse to be substantially different from expectations.

All this adds weight to the evidence that the dSph galaxies of the Milky Way possess dark matter cores. This evidence includes the survival of kinematically cold substructure in Ursa Minor (Kleyna et al. 2003), the longevity of the globular cluster population in Fornax (Goerdts et al. 2006; Sánchez-Salcedo et al. 2006; Cole et al. 2012), as well as the kinematics of stars in Sculptor (Battaglia et al. 2008; Amorisco & Evans 2012a; Agnello & Evans 2012) and in Fornax (Walker & Peñarrubia 2011). There is no direct evidence in favour of a dark matter cusp in any dSph.

The nature of the central parts of dark haloes of dSphs is important for two reasons. First, indirect detection experiments are monitoring the sky for signals of the expected γ ray emission produced by pair annihilation of weakly interacting dark matter particles. For example, the Large Area Telescope (LAT) on the Fermi satellite has constrained the integral γ ray flux from 14 dSphs to place limits on the annihilation cross-section (Abdo et al. 2010; Ackermann et al. 2011). The beam-size of the LAT is comparable to the angular half-light radius of most dSphs ($\sim 0.5^\circ$). In turn, this is comparable to the angular scale where uncertainties from the dark matter profile on the J factor are minimized (Walker et al. 2011; Charbonnier et al. 2011). Therefore, whether cored or cusped models are used makes only modest differences to the interpretation of the Fermi LAT data. However, arrays of atmospheric Cerenkov telescopes like MAGIC and HESS (e.g., Aleksić et al. 2011; Abramowski et al. 2011) provide superior angular resolution, and now the existence of a dark matter core rather than a cusp substantially reduces the expected γ ray flux (e.g., Evans et al. 2004).

Secondly, it is a unique prediction of cold dark matter theories that the centres of dark haloes are cusped. The dSphs of the Milky Way are overwhelmingly dark matter dominated, and so provide natural testing grounds for assessing this hypothesis. The finding that the haloes of at least some of the dSphs are cored may be interpreted in one of two ways. Either it provides evidence for warm dark matter particles which – judging from the phase space density in the Fornax core – have mass ~ 0.5 keV (Dalcanton & Hogan 2001). Or, it provides evidence that baryonic processes such as supernovae feedback or episodic mass loss or in-fall have modified the pristine dark matter cusp. There is no shortage of suggestions of processes that could eradicate the cusps (see e.g. Read & Gilmore 2005; Cole et al. 2011; Pontzen & Governato 2012). The increasing size and richness of datasets on the dSphs, combined with the increasing sophistication of analysis tools, gives hope to the suggestion that observational data may soon allow us to discriminate between some of these possibilities.

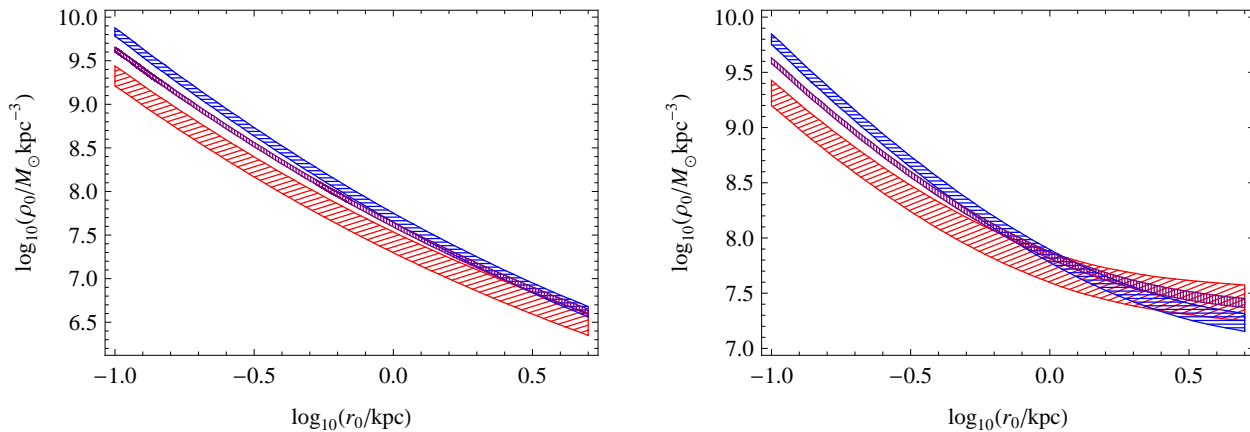


Figure 3. Left panel: virial stripes for the three subpopulations embedded in an NFW gravitational potential. Right panel: virial stripes for the three subpopulations embedded in a Burkert gravitational potential. In both panels stripes are associated with $1\text{-}\sigma$ regions and color coding is the same as in Fig. 1 and 2.

ACKNOWLEDGMENTS

NA and AA thank the Science and Technology Facility Council and the Isaac Newton Trust for financial support. We thank the anonymous referee for a critical reading of the manuscript.

REFERENCES

- Abdo, A. A., Ackermann, M., Ajello, M., et al. 2010, *ApJ*, 712, 147
- Abramowski, A., Acero, F., et al. 2011, *Astroparticle Physics*, 34, 608
- Agnello, A., & Evans, N. W. 2012, *ApJL*, 754, L39
- Ackermann, M., Ajello, M., Albert, A., et al. 2011, *Physical Review Letters*, 107, 241302
- Aleksić, J., Alvarez, E. A., Antonelli, L. A., et al. 2011, *JCAP*, 6, 35
- Amorisco, N. C., & Evans, N. W. 2011, *MN*, 411, 2118
- Amorisco, N. C., & Evans, N. W. 2012a, *MN*, 419, 184
- Amorisco, N. C., & Evans, N. W. 2012b, *MN*, in press (arXiv:1204.5181)
- Amorisco, N. C., & Evans, N. W. 2012c, *ApJL*, in press (arXiv:1206.6691)
- Battaglia, G., Helmi, A., Tolstoy, E., et al. 2008, *ApJL*, 681, L13
- Breddels, M. et al. 2012, arXiv:1205.4712
- Brooks, A. M., & Zolotov, A. 2012, arXiv:1207.2468
- Burkert, A. 1995, *ApJL*, 447, L25
- Charbonnier, A., Combet, C., Daniel, M., et al. 2011, *MN*, 418, 1526
- Cole, D. R., Dehnen, W., & Wilkinson, M. I. 2011, *MN*, 416, 1118
- Cole, D. R., Dehnen, W., Read, J. I., & Wilkinson, M. I. 2012, arXiv:1205.6327
- Coleman, M., Da Costa, G. S., Bland-Hawthorn, J., et al. 2004, *AJ*, 127, 832
- Coleman, M. G., Da Costa, G. S., Bland-Hawthorn, J., & Freeman, K. C. 2005, *AJ*, 129, 1443
- Coleman, M. G., & de Jong, J. T. A. 2008, *ApJ*, 685, 933
- de Blok, W. J. G., McGaugh, S. S., Bosma, A., & Rubin, V. C. 2001, *ApJL*, 552, L23
- Dalcanton, J. J., & Hogan, C. J. 2001, *ApJ*, 561, 35
- de Boer, T. J. L., Tolstoy, E., Hill, V., et al. 2012, arXiv:1206.6968
- Dubinski, J., & Carlberg, R. G. 1991, *ApJ*, 378, 496
- Evans, N. W., Ferrer, F., & Sarkar, S. 2004, *PRD*, 69, 123501
- Evans, N. W., An, J., & Walker, M. G. 2009, *MN*, 393, L50
- Goerdt, T., Moore, B., Read, J. I., Stadel, J., & Zemp, M. 2006, *MN*, 368, 1073
- Irwin, M., & Hatzidimitriou, D. 1995, *MN*, 277, 1354
- Jardel, J. R., & Gebhardt, K. 2012, *ApJ*, 746, 89
- Kleyna, J. T., Wilkinson, M. I., Gilmore, G., & Evans, N. W. 2003, *ApJL*, 588, L21
- Lokas, E. L. 2009, *MN*, 394, L102
- Macciò, A. V., Dutton, A. A., van den Bosch, F. C., et al. 2007, *MN*, 378, 55
- Navarro, J. F., Frenk, C. S., & White, S. D. M. 1997, *ApJ*, 490, 493
- Pontzen, A., & Governato, F. 2012, *MN*, 421, 3464
- Read, J. I., & Gilmore, G. 2005, *MN*, 356, 107
- Sánchez-Salcedo, F. J., Reyes-Iturbide, J., & Hernandez, X. 2006, *MN*, 370, 1829
- Strigari, L. E., Frenk, C. S., & White, S. D. M. 2010, *MN*, 408, 2364
- Teyssier, R., Pontzen, A., Dubois, Y., & Read, J. 2012, arXiv:1206.4895
- Wilkinson, M. I., Kleyna, J., Evans, N. W., & Gilmore, G. 2002, *MN*, 330, 778
- Walker, M. G., Mateo, M., & Olszewski, E. W. 2009, *AJ*, 137, 3100
- Walker, M. G., Mateo, M., Olszewski, E. W., et al. 2009, *ApJ*, 704, 1274
- Walker, M. G., Combet, C., Hinton, J. A., Maurin, D., & Wilkinson, M. I. 2011, *ApJL*, 733, L46
- Walker, M. G., & Peñarrubia, J. 2011, *ApJ*, 742, 20
- Wu, X. 2007, arXiv:astro-ph/0702233